applied sciences

MDPI

Article

Research on High-Speed Railway Subgrade Design Method Based on Energy Dissipation and Dynamic Stability Characteristics

Zongqi Bi [1,2,*], Yangsheng Ye [2,3], Degou Cai [1,2], Hongye Yan [1,2], Mingzhe Ouyang [1,2] and Ke Su [1,2]

[1] Railway Engineering Research Institute, China Academy of Railway Sciences Corporation Limited, Beijing 100081, China
[2] State Key Laboratory for Track Technology of High-Speed Railway, China Academy of Railway Sciences Corporation Limited, Beijing 100081, China
[3] China State Railway Group Corporation Limited, Beijing 100844, China
* Correspondence: bizongqitky@163.com

Abstract: The subgrade structure of high-speed railways is an important foundation for the safe and smooth operation of high-speed trains, and the scientific design of the subgrade structure provides a fundamental guarantee of its durability and technical economy. As, in the development of high-speed railways in China, higher speeds are being pursued, more requirements have been put forward for the dynamic stability of subgrade structures. To address this issue, this article focuses on the control requirements for the long-term stability of subgrade deformation, and various design methods for high-speed railway subgrade structures are presented. Considering the energy dissipation and dynamic stability characteristics of subgrade filling materials, the dynamic performance of coarse-grained soil filling materials in the bottom layer and graded crushed stones in the surface layer are revealed. The methods for determining the values of dynamic parameters such as the dynamic modulus and damping ratio are provided. Based on the dynamic shakedown theory, the stress–strain hysteresis characteristics of fillers and the variation law of dissipated energy are revealed. The correlation between unit volume dissipated energy and shakedown state under cyclic loading conditions is identified. A criterion for determining the critical shakedown state of high-speed railway subgrade structures based on equivalent unit volume dissipated energy is proposed, and a method for determining the design threshold of dynamic stress and dynamic strain is also proposed. The results show that the shakedown design critical values of equivalent unit volume dissipated energy in the bottom and surface layers of the foundation were between 0.0103~0.0133 kJ/m^3 and 0.0121~0.0149 kJ/m^3, respectively. The critical dynamic strain range was 0.8×10^{-3}~1.3×10^{-3}. On this basis, a high-speed railway subgrade design method based on energy dissipation and dynamic shakedown characteristics was developed. The results can provide theoretical support for the design of high-speed railway subgrade structures with different filling material alternatives and control standards.

Keywords: high-speed railway; subgrade filler; dynamics parameters; shakedown theory; dissipated energy; long-term deformation; design method

check for updates

Academic Editors: Igal Shohet and Paulo Santos

Received: 25 September 2024
Revised: 12 November 2024
Accepted: 13 November 2024
Published: 13 January 2025

Citation: Bi, Z.; Ye, Y.; Cai, D.; Yan, H.; Ouyang, M.; Su, K. Research on High-Speed Railway Subgrade Design Method Based on Energy Dissipation and Dynamic Stability Characteristics. *Appl. Sci.* **2025**, *15*, 734. https://doi.org/10.3390/app15020734

Copyright: © 2025 by the authors. Licensee MDPI, Basel, Switzerland. This article is an open access article distributed under the terms and conditions of the Creative Commons Attribution (CC BY) license (https://creativecommons.org/licenses/by/4.0/).

1. Introduction

The subgrade structure of high-speed railways provides an important foundation for the safe and smooth operation of high-speed trains, and the scientific design of the

subgrade structure is a fundamental guarantee of durability and technical economy. Finding an effective method for designing high-speed railway subgrade structures is a challenge that must be overcome to achieve high-precision deformation control and durability of service. The railway and soil system is a classical soil structure, and several studies have been implemented to clarify its mechanism [1–4].

Subgrade filling is used as the basic raw material for constructing the subgrade structure. Its mechanical characteristics and deformation evolution laws under the action of driving vibration are directly related to the overall durability and stability of the subgrade structure. Therefore, in the design of high-speed railway subgrade structures, the main focus is on the reasonable control of the structure under a working state and its long-term deformation under periodic dynamic loads. The current design method for high-speed railway subgrade structures in China adopts indicators such as the average dynamic strain of the subgrade bottom layer and the dynamic deformation of the surface layer, and the critical strain value is used as the design judgment criterion. Although the critical strain control value in current design mainly comes from typical test results and empirical values for fine-grained soil, it still essentially follows this design concept.

In recent years, research on the design control threshold of subgrade filling materials has mainly focused on the cumulative deformation of filling materials under cyclic loading, the influence of factors including the stress level [5,6], the number and frequency of cyclic actions [7–9], compactness [10,11], stress history [12–14], and different development modes and convergence characteristics. Heath et al. [15] and Cai et al. [16] classified the relationship curve between the cumulative plastic strain and the number of load actions as one of two types, the development type and decay type, based on the concavity and convexity of the curve in semi-logarithmic coordinates. Wang et al. [17] classified the cumulative plastic deformation curve as a stable, decay, or failure type and provided the critical cumulative strain between different states. Minassian [18] also classified the cumulative plastic strains under cyclic loading into three states based on the volumetric plastic strain. Jiao et al. [19] explored the concept of critical dynamic stress in soil and classified the cumulative strain characteristics into three categories: stable, failure, and critical. Nie et al. [20] also provided these three types of cumulative strain forms. Based on the linear relationship between cumulative strain and cyclic vibration frequency, an empirical formula for critical dynamic stress with confining pressure, moisture content, and static strength as variables was proposed. According to the characteristics of the cumulative deformation of subgrade filling under cyclic loading, Luo et al. [21] and Liu et al. [22] proposed four types: rapid stability, slow stability, slow failure, and rapid failure. They established a power law discrimination method based on the development of the cumulative deformation rate and explored the control principles and technical conditions of the deformation state of railway subgrade structures. Ye et al. [23] and Zhang et al. [24] proposed a high-speed railway subgrade structure analysis and strain control design method based on critical volume effect strain to control the deformation and pore pressure accumulation under repeated loads.

During the hundred-year service life of the high-speed railway, it will face the long-term impact of billions of dynamic load cycles. In theoretical methods applicable to low-cycle load conditions, there are often difficulties in analyzing the long-term deformation mode under such high-cycle loading with respect to efficiency and accuracy because of difficulties including testing and simulation costs, calculation redundancy errors, and obtaining corresponding parameters.

As a critical state method different from conventional elastic–plastic incremental analysis, the shakedown theory provides an effective approach to predicting structural safety and evaluating long-term deformation and stability. It was first proposed by Melan et al. [25] and further developed by Maier [26], Ceradini [27], and Polizzotto [28]. The shakedown

theory gives the design criteria from the perspective of the ability of the structure to resist external complex loads to maintain long-term stability. Compared with the traditional method, shakedown analysis does not need an accurate load and time history. Through shakedown analysis, different deformation accumulation trend lines and critical conditions can be distinguished; thus, the shakedown properties of materials can be determined. In recent years, the shakedown theory has been widely used in geotechnical engineering, such as in pavement rutting deformation [29], the foundation bearing capacity of offshore platforms [30], slope stability [31], and ballastless track structures [32]. Shakedown load has gradually become an important basis for the plastic failure criterion in the code for engineering strength design, which provides a powerful tool for the selection of the critical load and the prediction and control of long-term deformation in high-speed railways under long-term dynamic loads.

In recent years, scholars have carried out many studies on the development of permanent deformation and the shakedown critical threshold of geotechnical materials and have proposed different shakedown classification bases and critical shakedown criteria. Werkmeister et al. [33] took the change value of axial cumulative plastic strain as the basis for the classification of dynamic behavior types, and the strain rate of representative stages in the loading curve was used to distinguish the deformation trend and the types of shakedown state. On this basis, Chen et al. [34] used the slope of the subcycle compression stage in the semi-logarithm curve of plastic strain loading times as the basis for dividing the shakedown state. Xiao et al. [35] used the curves of cumulative strain, strain rate, and resilient modulus as the basis for judging the shakedown type. Moreover, Xiao et al. [36] proposed three discrimination types for railway ballast materials, i.e., shakedown state, plastic creep state, and incremental failure state. Zheng et al. [37] proposed a different stage division method of permanent deformation based on the Savitzky–Golay filtering method according to the development of axial cumulative plastic strain in coarse-grained soil subgrade filler under different dynamic stress paths, and the effect of cyclic confining pressure was taken into consideration. Wang et al. [38] characterized the plastic deformation and shakedown behavior of subgrade soil in seasonal frozen regions, and proposed a shakedown standard based on the evolution of the accumulative plastic strain rate. Wang et al. [39,40] also classified the permanent strain properties with strain rate $\Delta\varepsilon_p$, $5000 - \Delta\varepsilon_p$, 3000, and the variation in the loading frequency was considered. Liu et al. [41,42] investigated the long-term deformation of unbound granular materials through cyclic triaxial tests and DEM analysis and proposed a negative-power function to characterize the variation in the permanent strain rate. Martins et al. [43] obtained the threshold between the plastic shakedown and the plastic creep shakedown behavior of unreinforced and fiber-reinforced stabilized soils by using the absolute axial strain. Buddhima et al. [44] determined three types of unfavorable stress conditions: (i) excessive plastic settlement, (ii) progressive shear failure, and (iii) subgrade fluidization, and used stress–strain patterns in the p′-q plane with the critical number of cycles to distinguish them. Zhang et al. [45] established a prediction model for the plastic shakedown limit of reinforced coarse-grained soils by integrating the additional confining pressure of the geogrid or geocell into the criterion for unreinforced specimens. Li et al. [46] proposed a classification criterion based on the difference in resilient strain between the first and second loading stages $\Delta\varepsilon_{e,1-2}$, considering the intermittent loading. They also presented a simpler method of identifying the deformation behaviors of subgrade filler, based on the stable value of resilient strain. Zhai et al. [47] and Xu et al. [48] studied the dynamic stability of a coarse-grained subgrade soil and established a gray correlation model to analyze the correlation between the type of cumulative strain curve and confining pressure, dynamic stress, etc. A *BP* neural network model to predict the critical dynamic stress was proposed, and an empirical formula for

the critical dynamic stress considering the effect of confining pressure and water content was given. Bi et al. [49] proposed an improved thermo-parameter method (*TPM*) to carry out dynamic shakedown analysis on railway subgrade, which can be used in the *FEM* analysis. Lei et al. [50] proposed a lower-bound shakedown analysis method for pavement systems under moving traffic loadings, considering pavement roughness. The effects of moving speed, wavelength irregularity, and the modulus and pavement thickness on the shakedown limit were discussed. The above methods have yielded valuable conclusions in different types of geotechnical materials. However, the selection of the shakedown critical criterion mostly comes from the apparent law and correlation analysis of cumulative deformation and strain rate curve shape in the test. The theoretical correlation between the deformation stability and shakedown critical state of different types of subgrade fillings needs to be further studied.

Based on shakedown theory and from the perspective of energy, this paper studies the plastic strain accumulation characteristics, cyclic stress–strain hysteresis characteristics, and dissipation energy evolution law for six types of typical subgrade coarse-grained soil fillings, and the relationship among long-term deformation trend, shakedown critical state, and dissipation energy is established. A criterion for determining the shakedown critical state based on the equivalent unit volume dissipation energy and a method for determining the corresponding control threshold are proposed. The research results can provide theoretical support for the shakedown design of high-speed railway subgrade.

2. Dynamic Triaxial Test of Typical Coarse-Grained Soil Filler for High-Speed Railway Subgrade

2.1. Test Equipment and Specimen Preparation

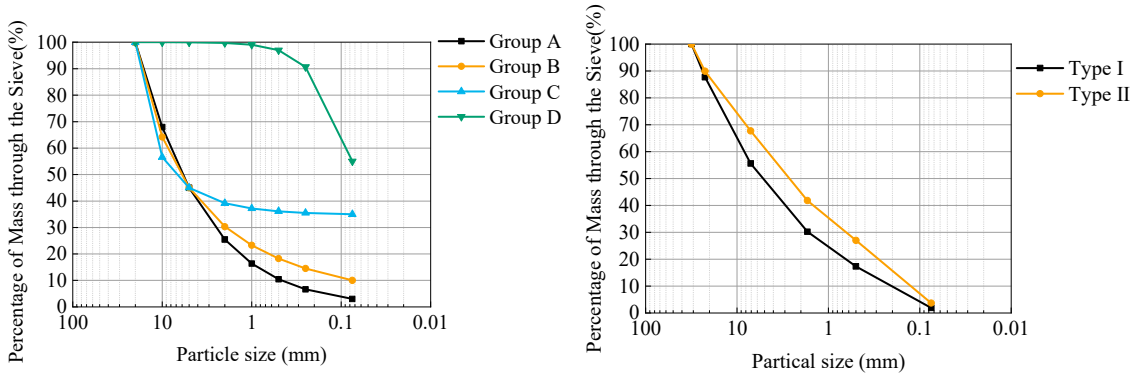
This paper mainly studies the long-term deformation and energy dissipation law under cyclic loading for the surface layer and bottom layer of high-speed railway subgrade. The test was carried out using a large diameter triaxial test system, as shown in Figure 1. It includes a dynamic loading system, pressure chamber, confining pressure control system, data acquisition and control operation system, etc. The dynamic loading system is controlled by the closed loop of the servomotor. The axial force is 0~64 kN; the frequency is 0~5 Hz. The displacement stroke and control accuracy are ±100 mm and 0.20 μm, respectively. The pressure chamber is suitable for triaxial specimens with a maximum diameter of 300 mm, to meet the requirements for the configuration size of coarse-grained soil specimens.



Figure 1. Dynamic triaxial test system.

The triaxial specimens used in the test were prepared according to the typical coarse-grained soil filler grading of high-speed railway subgrade in China. According to the code

for the design of railway ground structures (TB 10001-2016) [51], the grading curves of filler specimens were determined, including type I- and type II-graded crushed stones for the surface layer of subgrade and group A, B, C, and D fillers for the bottom layer of the subgrade bed, with a total of six types of grading curves. The triaxial specimen used in the test was 150 mm in diameter and 300 mm in height. According to the requirement that the maximum particle size not be greater than 1/6~1/5 of the sample diameter, the equivalent substitution method was used to adjust the particle grading of the original soil sample, and the maximum particle diameter was set as 20 mm. The grading curve for each group is shown in Figure 2. The samples were mixed according to the grading requirements and were sealed and cured for 24 h to ensure a uniform water content, then the samples were compacted in five layers in the membrane cylinder. According to the compaction standard for the subgrade bed of a high-speed railway [51], the moisture content of the sample was configured according to the optimal moisture content, and the compaction degree was controlled by 0.97 of the surface layer and 0.95 of the bottom layer in the subgrade bed.



(**a**) Coarse-grained soil fillers for the bottom layer. (**b**) Graded crushed stones for the surface layer.

Figure 2. Gradation curves of specimens.

2.2. Test Process

Before the dynamic load was applied, the initial confining pressure condition was first applied to simulate the initial stress state of the filler at different depths of the subgrade bed under the static load. According to the layered thickness of the standard subgrade structure, the surface layer and the surface, center, and bottom position of the bottom layer were taken for research. The corresponding test confining pressures were set at 5 kpa, 15 kpa, 30 kPa, and 60 kPa, respectively. For type I and type II crushed stones in the surface layer, the confining pressures were 5 kPa and 10 kPa, respectively. After the confining pressure was applied, consolidation and stabilization were carried out for at least 6 h.

In the test, multi-stage loading was adopted. The first-level load amplitude $l_{d,1}$ = 0.05 kN, the second-level load amplitude $l_{d,2}$ = 0.1 kN, the subsequent amplitude increment of each level was Δl_d = 0.1 kN, the dynamic stress amplitude increment of each level was about 10 kPa, and the number of load cycles of each level ΔN was 10^4. The test load simulated the train load, and the effect of two bogies in two adjacent carriages on the subgrade represented a loading cycle [52,53]. When the train speed was 400 km/h, the corresponding frequency was about 4.5 Hz. The loading frequency was 5 Hz, which corresponded to the load frequency caused by the adjacent bogie when the train passed through at the speed of 450 km/h.

The test control conditions are shown in Table 1. This study mainly focused on the influencing factors such as the confining pressure level σ_3, dynamic stress level σ_d, and loading times N. The experimental objective was to obtain the cumulative deformation law of different fillers under dynamic action, and an increasing load form was used to elucidate the critical conditions for the specimens to transition from a stable to unstable state.

Table 1. Test scheme.

Group	No.	σ_3 (kPa)	$l_d = \sigma_d \times A_s$ * (kN)	ΔN * (—)
A	M01~M04	5, 15, 30, 60	$l_{d,i} = l_{d,i-1} + \Delta l_d$, $i > 2$ $l_{d,1} = 0.05$, $l_{d,2} = 0.1$ $\Delta l_d = 0.1$	$\Delta N = 1 \times 10^4$
B	M05~M08	5, 15, 30, 60		
C	M09~M12	5, 15, 30, 60		
D	M13~M16	5, 15, 30, 60		
Type I	M17~M18	5, 10		
Type II	M19~M20	5, 10		

* l_d is the amplitude of the axial force applied in the experiment; $l_{d,i}$ is the amplitude of the axial force applied by the i-th level in graded loading; Δl_d is the increase in the amplitude of axial force at each stage of graded loading; A_s is the area of the specimen subjected to axial force, taken as 0.017 m^2; and ΔN is the number of cycles applied to each level in hierarchical loading.

2.3. Methodological Approach

Based on the results of the triaxial tests, the relationship between cumulative deformation and the number of cyclic loadings was established. From the generated curves, the cumulative strain rate per unit cycle was computed, and its development trends throughout the loading process were analyzed. The shakedown theory was employed to differentiate the convergence of cumulative deformation and the cumulative strain rate.

The stress–strain relationship was derived from the test results, and hysteretic curves were constructed to analyze the evolution of hysteretic cycles across different deformation modes as the loading times increased. This analysis was also conducted according to shakedown theory. Furthermore, the energy dissipation index per unit volume was applied for quantitative assessment and calculation, aiming to determine the cumulative energy dissipation behavior of the filler under various deformation modes.

By employing the kinematic shakedown theorem, this study constructed a correlation between energy dissipation and the deformation stability of materials. An index named "equivalent dissipated energy per unit volume" was introduced to evaluate the critical thresholds for three types of shakedown states in fillers. Building on this framework, the critical dynamic stress and strain for different types of fillers were presented. In addition, through data fitting, calculation formulas and reference values for the packing shakedown critical thresholds under varying confining pressures were provided.

The research framework is shown in Figure 3. The blue arrow indicates the sequence of the research methods used and the source relationship of the results. The dotted box represents the set of three types of shakedown states, which can be obtained from the test results and shakedown analysis.

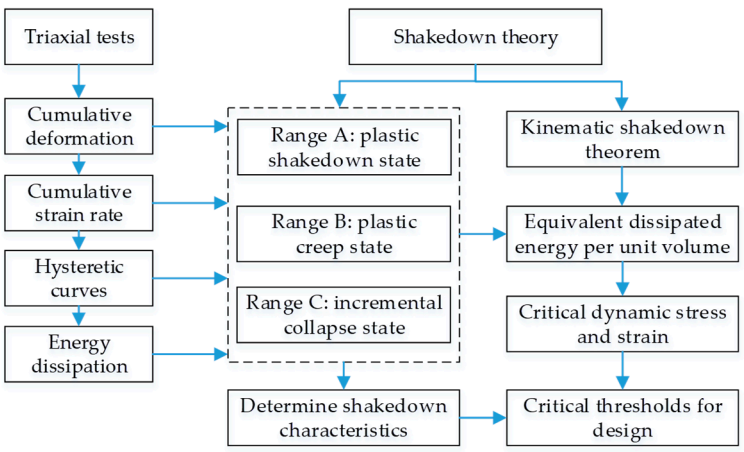


Figure 3. Research framework.

3. Long-Term Deformation and Energy Dissipation Characteristics

3.1. Long-Term Cumulative Deformation and Shakedown Characteristics

Based on shakedown theory, the stress–strain cycles of subgrade filler present different development laws under different dynamic loadings, as shown in Figure 4. The curve with an arrow indicates the load–strain relationship with the loading and unloading cycle, its direction indicates the load path, and the dashed section indicates several cycles that are not shown. When the stress–strain cycle stabilized in the initial few cycles, the accumulated strain rate continuously decreased, while the hysteresis curve closed or showed an approximate linear relationship; thus, no new deformation accumulation occurred, and it was called the "plastic shakedown state" (Range A). When the hysteresis loop gradually developed in the direction of strain accumulation, as the strain rate still increased in a high cycle, it exhibited a "plastic creep state" (Range B). When the hysteresis curve did not close and rapidly developed towards strain accumulation, the strain rate exhibited an increasing trend even in a low cycle, and a sudden increase in deformation occurred in a short duration, which was called "incremental collapse state" (Range C).

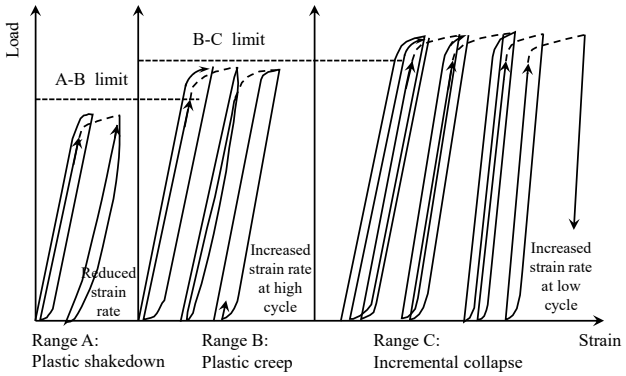
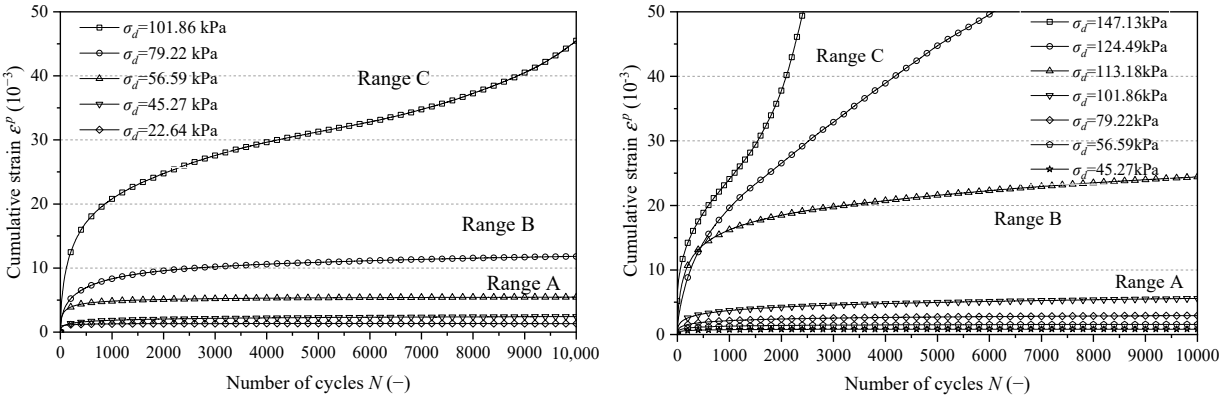
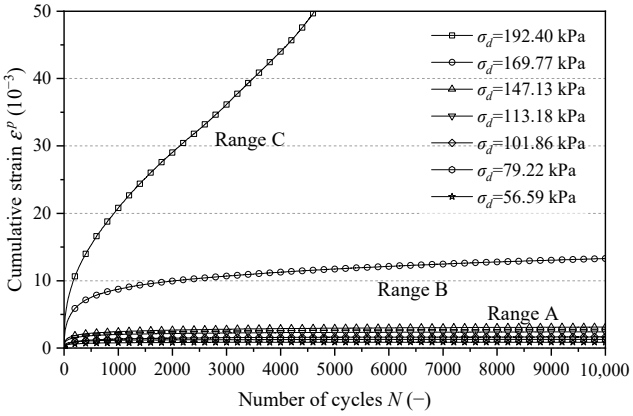


Figure 4. Stress–strain relationship and shakedown characteristics under cyclic loading.

The long-term deformation development of subgrade filler under different cyclic stress levels was obtained. Taking the cumulative deformation and strain rate curves of group B under different dynamic stress amplitudes as an example, the results under the three confining pressures of 15 kPa, 30 kPa, and 60 kPa are shown in Figures 5 and 6. The test conditions correspond to the typical confining pressure at the surface, center, and bottom position in the bottom layer of subgrade.

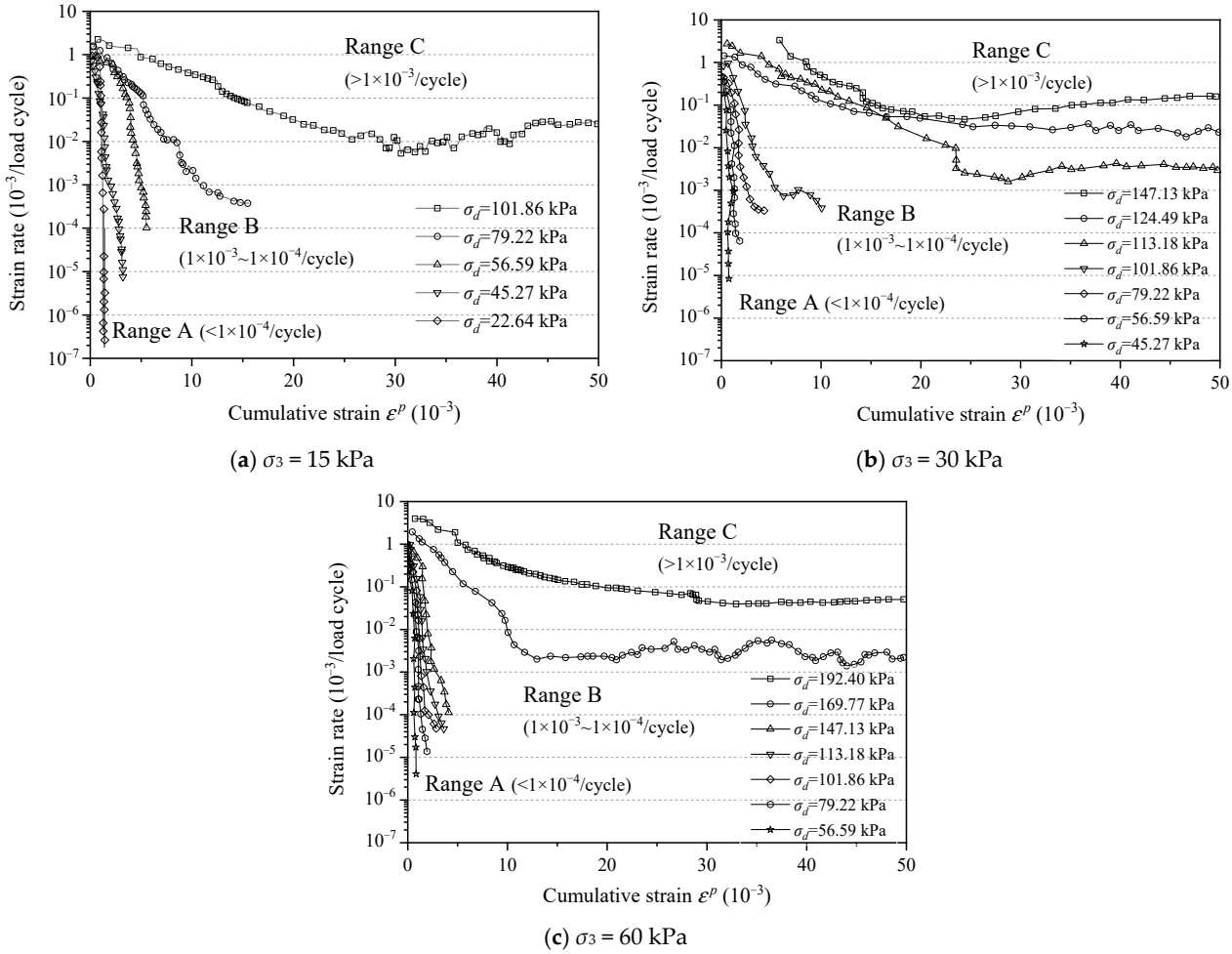


(**a**) σ_3 = 15 kPa (**b**) σ_3 = 30 kPa



(**c**) σ_3 = 60 kPa

Figure 5. Cumulative deformation curves under different dynamic stress amplitudes (Group B).



(**a**) σ_3 = 15 kPa

(**b**) σ_3 = 30 kPa

(**c**) σ_3 = 60 kPa

Figure 6. Variation in strain rate with cumulative strain under different dynamic stress amplitudes (Group B).

Under different dynamic stress amplitudes, there are obvious differences in the cumulative law of the permanent strain of the filler. To be specific, for Range A, when the dynamic stress amplitude was small enough, the accumulation curve remained stable for a long time after a small amount of strain accumulation in the initial several cycles, and no new deformation accumulation occurred. For Range B, with the gradual increase in the dynamic stress amplitude, the development rate of the strain increased gradually. In this process, new deformation accumulation occurred in each external load cycle, and the permanent deformation showed a continuous and slow growth trend. For Range C, when the dynamic stress amplitude exceeded a certain limit, the permanent deformation curve showed an upward trend, a large cumulative strain occurred in a very short time ($\varepsilon^p > 5\%$), and the sample was damaged. According to the development trend of cumulative strain, even at small stress levels, all samples showed plastic strain, which indicated that the actual working state of railway subgrade filler was usually not a purely elastic state.

Corresponding to the cumulative strain, the strain rate can further reflect the development trend and different stable states of the above three types of strain accumulation. The variation in strain rate with cumulative strain under different dynamic stress amplitudes is shown in Figure 5. The strain rates of specimens were also divided into three ranges. Taking the result of confining pressure σ_3 = 30 kPa as an example, the strain rate in Range A decreased rapidly with the increase in accumulated strain, reaching below 1×10^{-5}/cycle, without continuous deformation accumulation. The strain rate in Range B decreased as the accumulated strain increased, with a certain deflection at the end of the curve, and

finally stayed between 1×10^{-3}~1×10^{-4}/cycle. The strain rate in Range C decreased slightly with the increase in accumulated strain and finally maintained at a high level (0.1~0.01/cycle). With the continuous increase in permanent deformation, the rate further increased and finally the cumulative strain exceeded the maximum strain (5%), which was considered as having reached a critical state.

3.2. Energy Dissipation Characteristics

The long-term stability or performance deterioration of high-speed railway subgrade structures under dynamic action is closely related to the change in its internal energy. Energy dissipation is an essential property of geotechnical materials and reflects the process of weakening and the eventually loss of intrinsic strength during cyclic deformation [54,55]. The dissipated energy of the filler in each cycle represents the unrecoverable strain energy under the action of external force. While the dissipated energy is generated, plastic deformation and residual stress and strain gradually increase from the initial state. This change can be understood as irreversible deterioration or damage caused by energy dissipation, which causes the filler to change from a stable state to an unstable state.

As shown in Figure 7, in the stress–strain hysteresis loop, the area surrounded by the loading section, the vertical dashed line, and the transverse axis is the unit volume energy, indicating the work carried out by the external force on the sample. The area around the unloading section and the transverse axis is the elastic energy per unit volume. The area difference in the loading and unloading curve is the dissipation energy per unit volume, that is, the area of the hysteresis loop. The dissipated energy per unit volume U^{d} is defined as

$$\begin{aligned} U^{\mathrm{d}} &= U - U^{\mathrm{e}} = \int \sigma \mathrm{d}\varepsilon - \int \sigma' \mathrm{d}\varepsilon' = \\ &\sum_{loading} (\sigma_i + \sigma_{i+1})(\varepsilon_{i+1} - \varepsilon_i)/2 - \\ &\sum_{unloading} (\sigma'_i + \sigma'_{i+1})(\varepsilon'_{i+1} - \varepsilon'_i)/2 \end{aligned} \tag{1}$$

where U is the total unit volume energy, U^{e} is the unit volume elastic energy, σ and ε are the stress and strain of the loading section, σ' and ε' are the stress and strain of the unloading section, and σ_i and ε_i are the stress and strain of segment i after discretization.

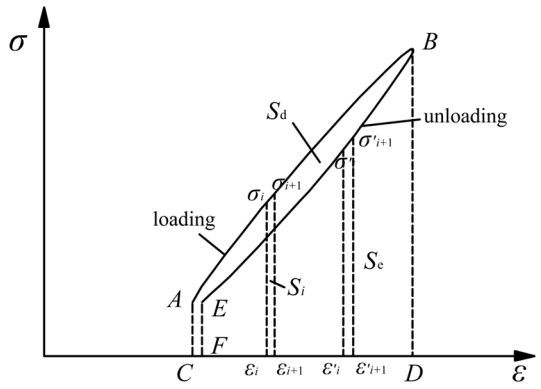


Figure 7. Hysteresis loop and energy dissipation under cyclic load.

The typical stress–strain hysteresis curves are in accordance with the three dynamic shakedown states, as shown in Figure 8. For Range A, the shape of the hysteretic loop at each stage was approximately linear, and the stress–strain relationship showed elastic behavior. This indicated that there was almost no new plastic dissipated energy generated in each cycle. For Range B, the shape of the hysteresis loop presented a thin crescent shape with a small hysteresis loop area. A certain amount of plastic dissipated energy was generated in each cycle, but the overall shape of the hysteresis loop did not change with the

development of the loading stage, indicating that the cumulative incremental rate of plastic strain was a relatively stable constant. For Range C, the hysteresis loops at each stage exhibited a wide crescent shape, with a strongly nonlinear stress–strain relationship. The hysteresis loop area was large, and the deformation of the specimen accumulated rapidly.

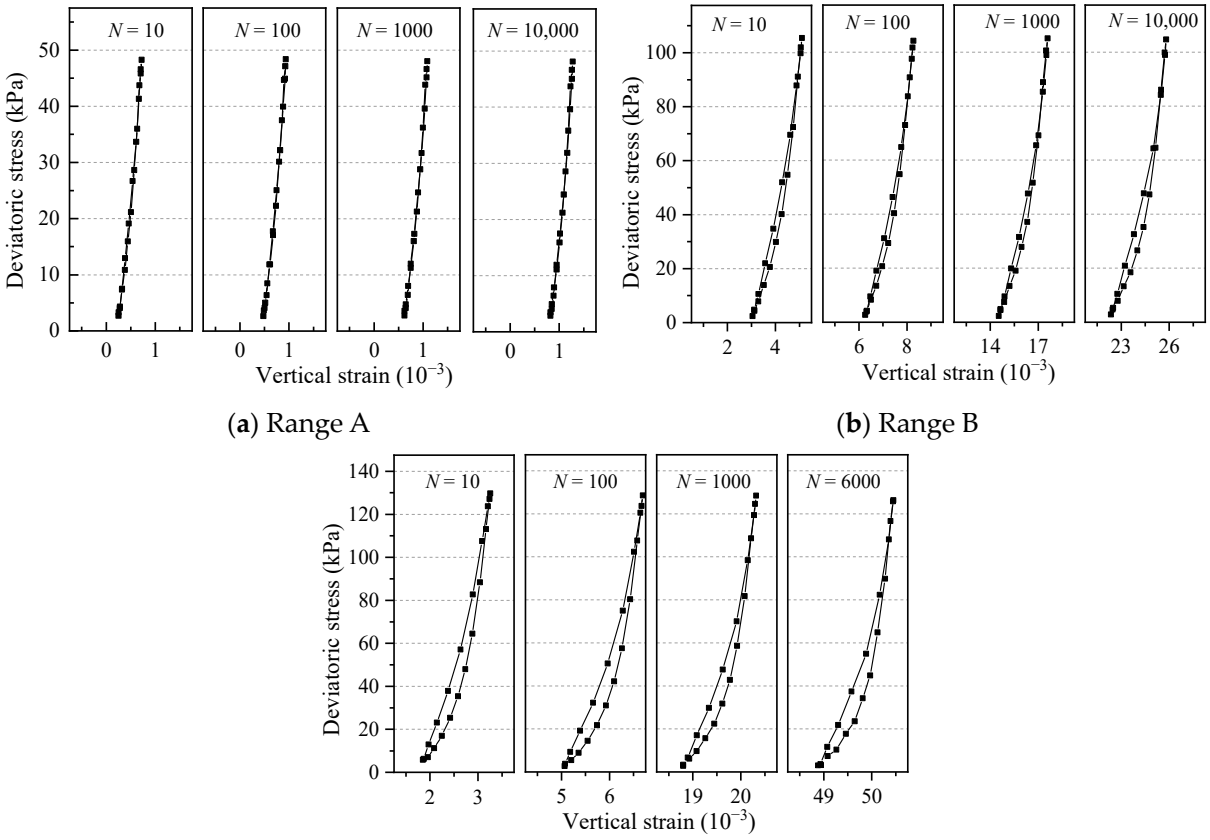
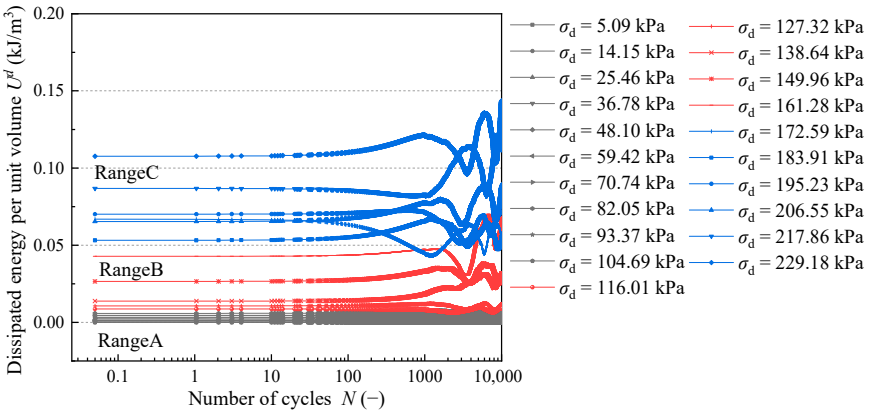


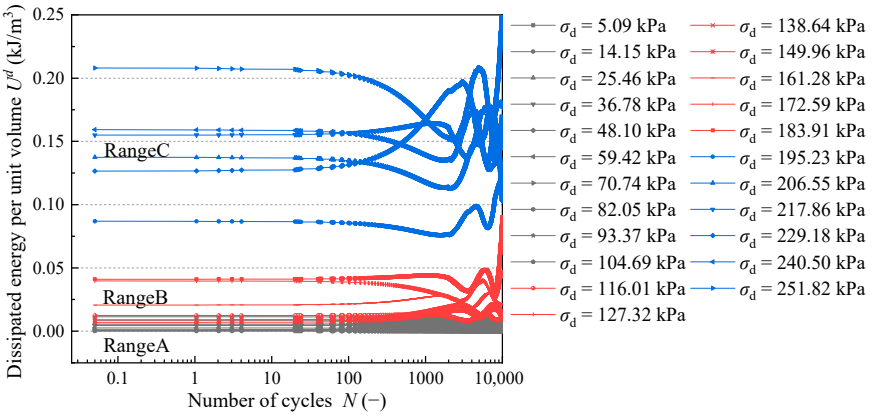
Figure 8. Stress–strain hysteresis curves under different dynamic shakedown states.

The variation curves of the dissipated energy per unit volume U^d obtained by Formula (1) with the number of cycles are shown in Figure 9. Taking Group B as an example, the values of U^d in Range A remained at a low level, about 0~0.01 kJ/m^3. In Range B, the values of U^d were approximately 0.01~0.05 kJ/m^3, showing a slight upward trend after a certain number of cycles. The values of U^d in Range C were greater than 0.05 kJ/m^3, with significant fluctuations or a significant increase with the increase in loading cycles. The final failure reached around 0.15~0.25 kJ/m^3.

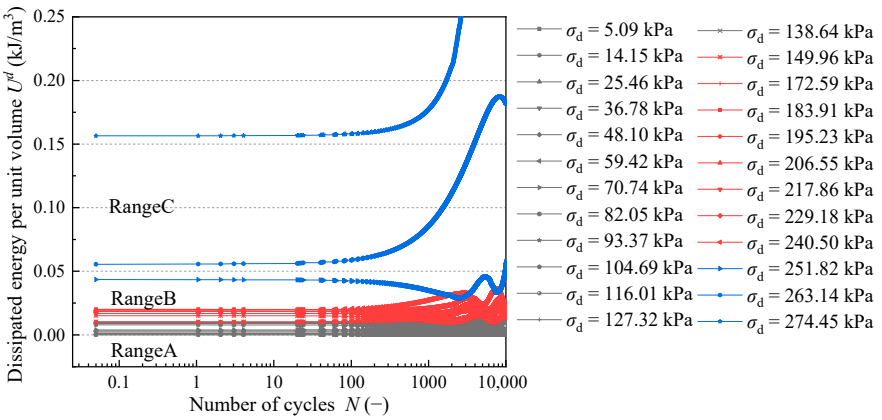
The results showed a good correspondence between the energy dissipation characteristics of fillers and the shakedown states exhibited by stress–strain behavior. For the plastic shakedown state, several cycles generated very little plastic dissipation energy, which was basically manifested as recoverable elastic energy in subsequent cycles. The plastic creep state corresponded to a higher level of dissipated energy, which gradually increased in high cycles. In the incremental collapse state, the dissipated energy remained at a high level, which was related to the irreversible deformation of the filler that occurred in a short period of time. As mentioned above, the magnitude and variation in dissipated energy showed significant differences, which can serve as relevant criteria for evaluating the shakedown states.



(**a**) σ_3 = 15 kPa



(**b**) σ_3 = 30 kPa



(**c**) σ_3 = 60 kPa

Figure 9. Variation in dissipated energy per unit volume with the number of cycles.

4. Control Threshold for Design Based on Dynamic Shakedown Characteristics

4.1. Criterion of Shakedown State Based on Dissipated Energy per Unit Volume

For the design of subgrade structures for high-speed railways, in order to ensure the long-term durability and stability of subgrade filler under traffic loading, it is necessary to keep it in a shakedown state where the deformation can converge and stabilize in a short time. When the total strain is small enough, the plastic shakedown state (Range A) is allowed, while the Range C state is strictly prohibited. Therefore, from the perspective of controlling the shakedown state of the subgrade structure, it is necessary to clarify the critical criteria between the three ranges and then put forward the design control thresholds.

According to the concept of the "kinematically admissible strain rate" of the kinematic shakedown theorem [56,57], if the external force power is not greater than the internal plastic dissipation power in a time period $0 < t < T$, then the object is stable, as shown in Equation (2).

$$\int_0^T P_a(t)\dot{u}_a^*(t)\mathrm{d}t \le \int_0^T \int_V \sigma_{ij}^* \dot{\varepsilon}_{ij}^{*p} \mathrm{d}V\mathrm{d}t \tag{2}$$

where $P_a(t)$ is the action of the external force, $\dot{u}_a^*(t)$ is the kinematically admissible velocity field, $\dot{\varepsilon}_{ij}^{*p}$ is the plastic strain rate, and σ_{ij}^* is the stress associated with $\dot{\varepsilon}_{ij}^{*p}$ through the plastic flow law.

Based on the above theory, the dissipated energy per unit volume is taken as the basis for judging the critical thresholds of shakedown states. Considering the corresponding relationship between unit volume dissipation energy and different long-term deformation development modes, the main influencing factors are the magnitude of unit volume dissipation energy and its variation trend of divergence or convergence.

Therefore, the equivalent dissipated energy per unit volume $\overline{U}_{\mathrm{eq}}^{\mathrm{d}}$ is proposed as an index to judge the shakedown critical state, which is expressed as

$$\overline{U}_{\mathrm{eq}}^{\mathrm{d}} = \overline{U}^{\mathrm{d}} \cdot \left(1 + \frac{U_m^{\mathrm{d}} - U_{m/10}^{\mathrm{d}}}{U_m^{\mathrm{d}}}\right) \tag{3}$$

where $\overline{U}^{\mathrm{d}}$ is the mean value of dissipated energy per unit volume, which is the influence term reflecting the value of dissipated energy. U_m^{d} is the final unit volume dissipative energy corresponding to the maximum cycle number m; $U_{m/10}^{\mathrm{d}}$ is the unit volume dissipative energy corresponding to the representative cycle number $m/10$. The dimensionless influence term in brackets reflects the rising trend in dissipated energy.

The values of $\overline{U}_{\mathrm{eq}}^{\mathrm{d}}$ under different confining pressures and dynamic stresses are illustrated in Figure 10. The threshold lines were obtained by calculating the limit values $\lambda_{\mathrm{A-B}}$ and $\lambda_{\mathrm{B-C}}$, and data points of $\overline{U}_{\mathrm{eq}}^{\mathrm{d}}$ were divided into three ranges according to different shakedown states.

The mean values of the upper and lower limits of $\overline{U}_{\mathrm{eq}}^{\mathrm{d}}$ in the critical region are taken as the critical lines to determine $\lambda_{\mathrm{A-B}}$ and $\lambda_{\mathrm{B-C}}$ and are represented by the red lines shown in the figure. The criterion for shakedown states based on the equivalent dissipated energy per unit volume can be given as follows:

$$\begin{cases} Range\ A : \overline{U}_{\mathrm{eq}}^{\mathrm{d}} < \lambda_{\mathrm{A-B}} \\ Range\ B : \lambda_{\mathrm{A-B}} < \overline{U}_{\mathrm{eq}}^{\mathrm{d}} < \lambda_{\mathrm{B-C}} \\ Range\ C : \overline{U}_{\mathrm{eq}}^{\mathrm{d}} > \lambda_{\mathrm{B-C}} \end{cases} \tag{4}$$

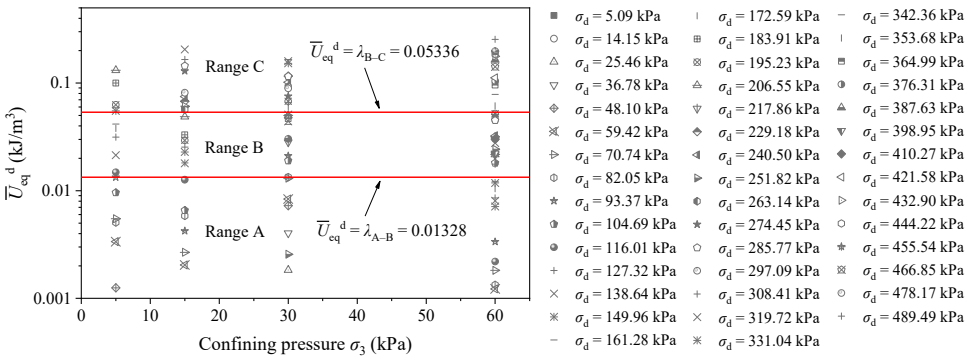
$$\lambda_{\mathrm{A-B}} = \frac{1}{2}\left(\overline{U}_{\mathrm{eq,Amax}}^{\mathrm{d}} + \overline{U}_{\mathrm{eq,Bmin}}^{\mathrm{d}}\right) \tag{5}$$

$$\lambda_{\mathrm{B-C}} = \frac{1}{2}\left(\overline{U}_{\mathrm{eq,Bmax}}^{\mathrm{d}} + \overline{U}_{\mathrm{eq,Cmin}}^{\mathrm{d}}\right) \tag{6}$$

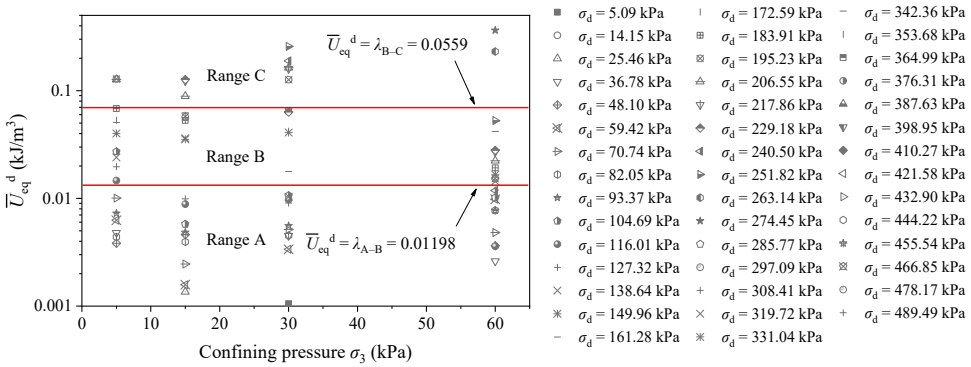
where $\lambda_{\mathrm{A-B}}$ and $\lambda_{\mathrm{B-C}}$ are critical values for equivalent dissipated energy per unit volume between Range A and B and Range B and C, respectively. $\overline{U}_{\mathrm{eq,Amax}}^{\mathrm{d}}$ is the max value of $\overline{U}_{\mathrm{eq}}^{\mathrm{d}}$ in Range A, $\overline{U}_{\mathrm{eq,Bmin}}^{\mathrm{d}}$ and $\overline{U}_{\mathrm{eq,Bmax}}^{\mathrm{d}}$ are the min and max value of $\overline{U}_{\mathrm{eq}}^{\mathrm{d}}$ in Range B. $\overline{U}_{\mathrm{eq,Cmin}}^{\mathrm{d}}$ is the min value of $\overline{U}_{\mathrm{eq}}^{\mathrm{d}}$ in Range C.

For the six types of typical high-speed railway subgrade fillers, the values of $\lambda_{\mathrm{A-B}}$ and $\lambda_{\mathrm{B-C}}$ are shown in Table 2. The values of $\lambda_{\mathrm{A-B}}$ and $\lambda_{\mathrm{B-C}}$ were in the range of 0.01~0.015 kJ/m^3

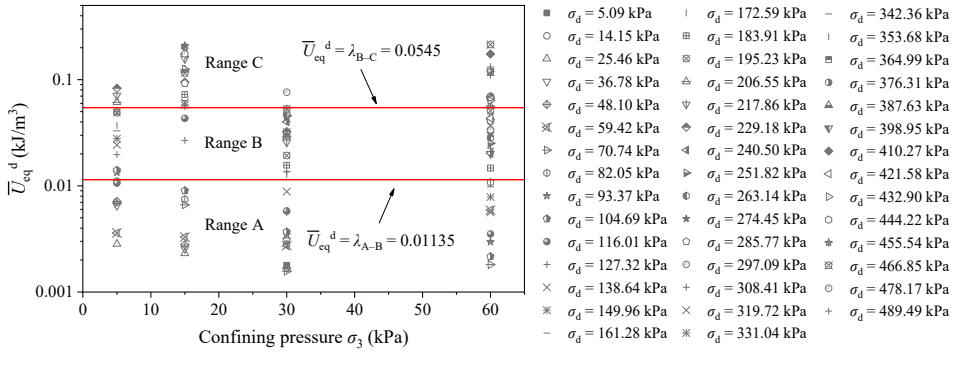
and 0.05~0.08 kJ/m^3, respectively. The critical values of the bottom layer were generally less than those of the surface layer. The values of $\lambda_{A–B}$ in groups A, B, C, and D decreased in turn, while the value of $\lambda_{B–C}$ did not change significantly. Different filler types and loading test conditions may affect the value, but the above criteria and determination methods are still applicable.



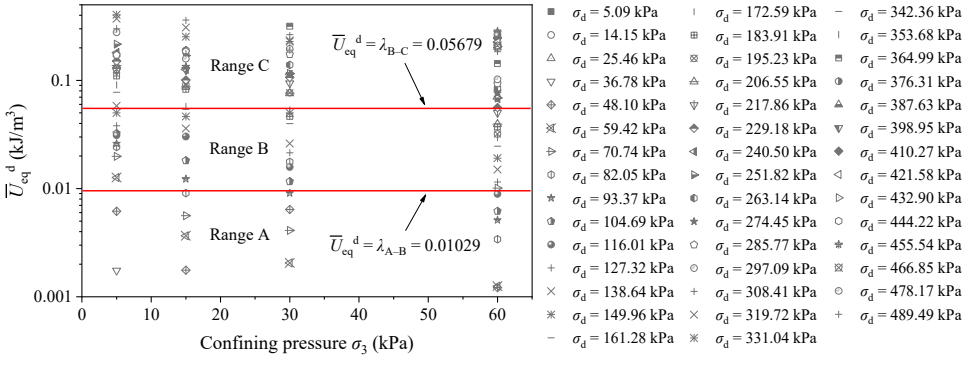
(**a**) Group A.



(**b**) Group B.

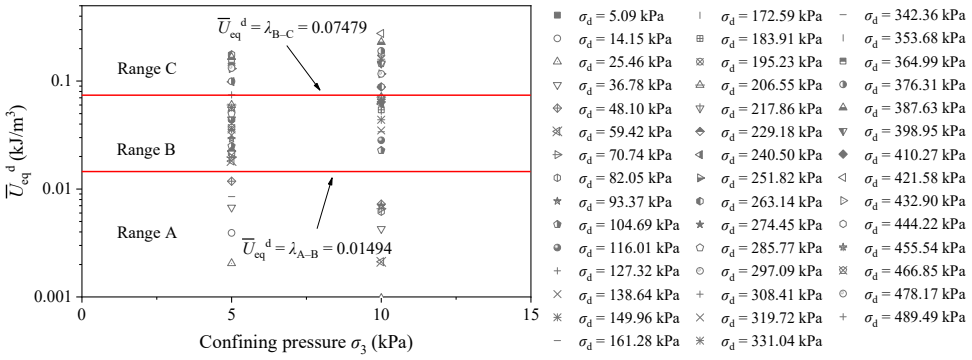


(**c**) Group C.

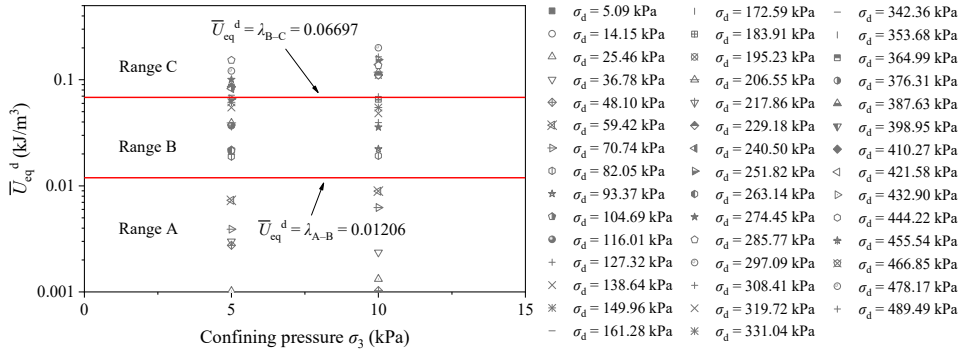


(**d**) Group D.

Figure 10. *Cont.*



(**e**) Type I.



(**f**) Type II.

Figure 10. Partition of dissipated energy per unit volume based on shakedown states.

Table 2. Critical values of equivalent dissipated energy per unit volume of different subgrade fillers.

Subgrade Filler	λ_{A-B} kJ/m^3	λ_{B-C} kJ/m^3
Group A of bottom layer	0.01328	0.05336
Group B of bottom layer	0.01198	0.05590
Group C of bottom layer	0.01135	0.05450
Group D of bottom layer	0.01029	0.05679
Type I of surface layer	0.01494	0.07479
Type II of surface layer	0.01206	0.06697

4.2. Shakedown Threshold of Typical Filling Materials

The relationship curves between the equivalent dissipated energy per unit volume and dynamic stress amplitude are shown in Figure 11, and the criterion lines for judging the critical value are marked in the figure (shown by the dotted lines). The intersection of the curve and the critical line represents the critical point of the shakedown critical state, that is, the thresholds of stress amplitude for Range A, B, and C under the corresponding confining pressures.

Similarly, for the dynamic strain amplitude under different test conditions, the relationship between its variation curves and the critical lines of unit volume dissipation energy are shown in Figure 12.

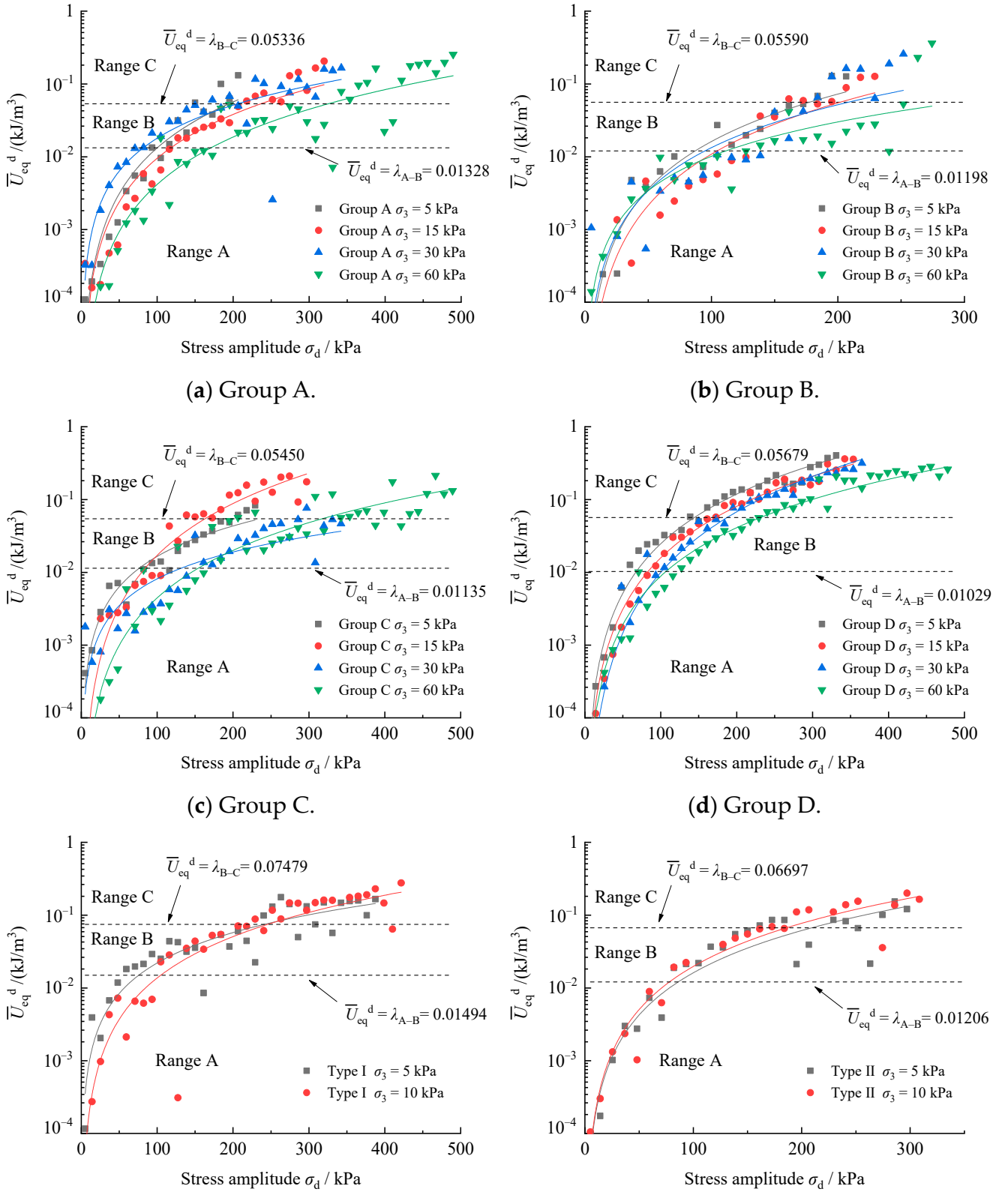


Figure 11. Variation curves for equivalent dissipated energy per unit volume with dynamic stress amplitude.

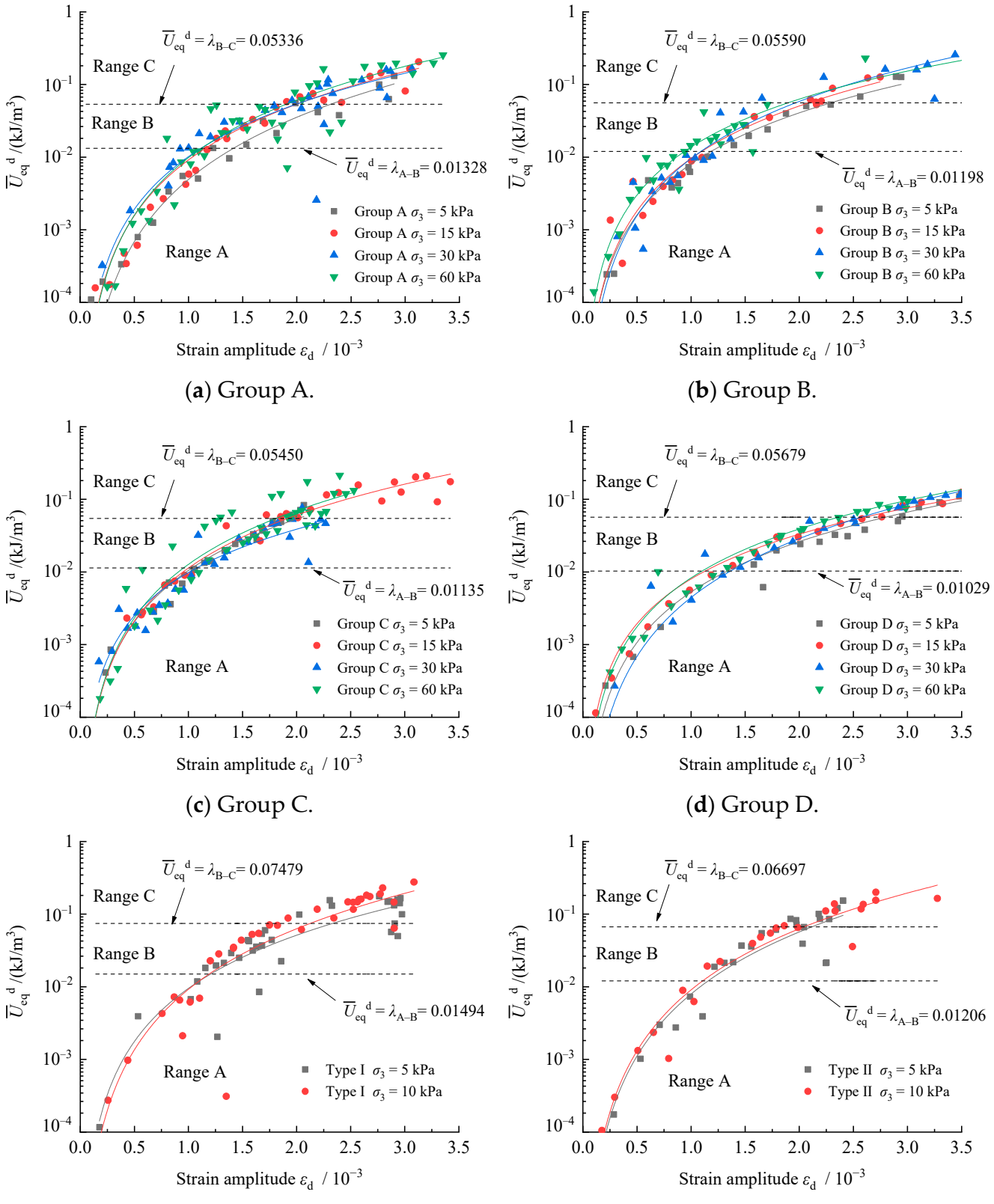
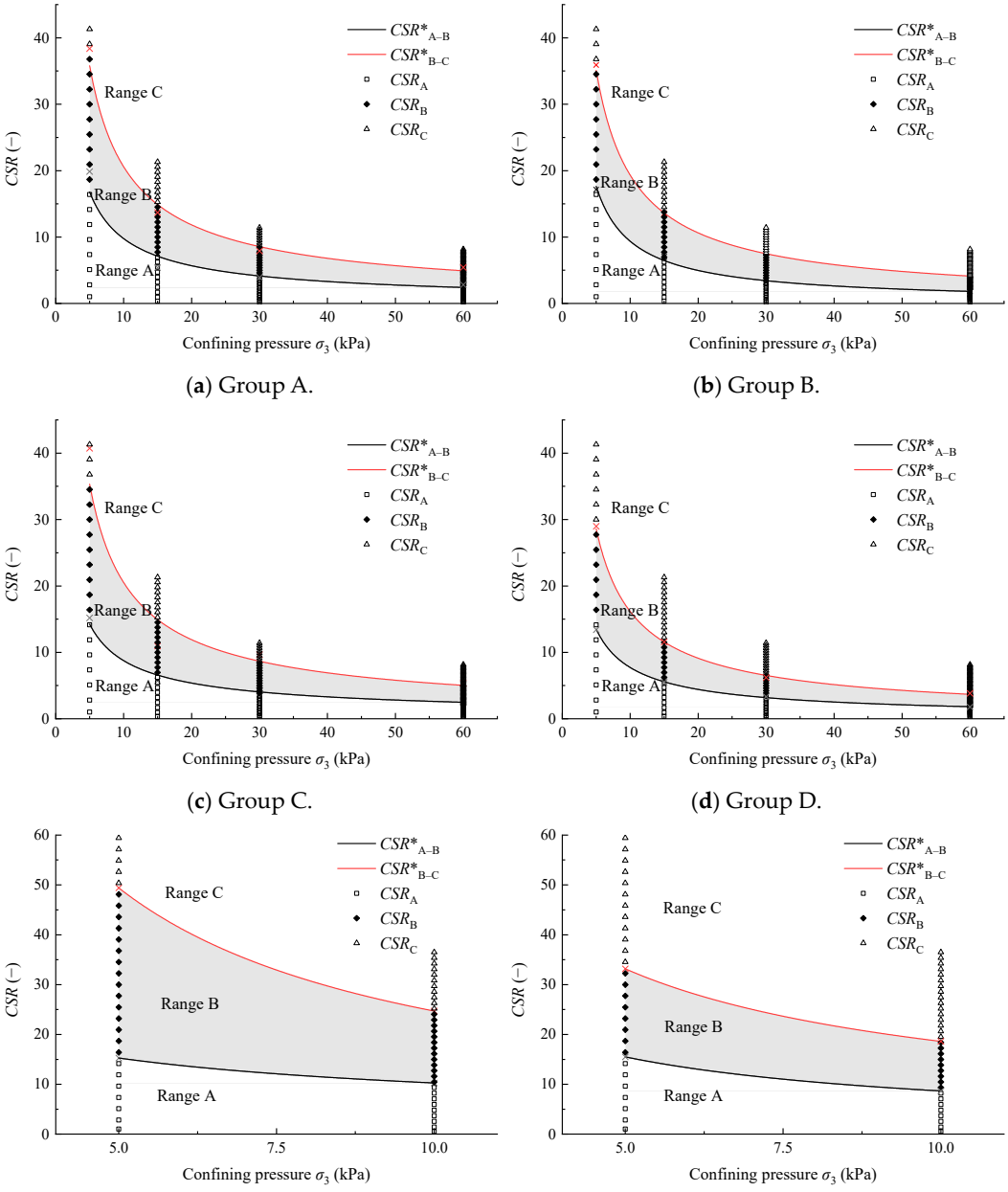


Figure 12. Variation curves for equivalent dissipated energy per unit volume with dynamic strain amplitude.

In order to define the dynamic stress shakedown critical threshold of coarse-grained soil filler for high-speed railway subgrade, the dimensionless parameter of the cyclic stress ratio (*CSR*) is used, which is expressed as follows:

$$CSR = \sigma_d / 2\sigma_3 \tag{7}$$

By substituting the critical value of dynamic stress amplitude σ_d in Figure 9 into Equation (7), the threshold curve of $CSR^*_{A–B}$ and $CSR^*_{B–C}$ can be obtained. As shown in Figure 13, the data points CSR_A at the lower left of the $CSR^*_{A–B}$ threshold curve are in the plastic shakedown state, the data points CSR_C at the upper right of the $CSR^*_{B–C}$ threshold curve are in the incremental collapse state, and the data points CSR_B in the shaded area between $CSR^*_{A–B}$ and $CSR^*_{B–C}$ are in the plastic creep state.



(**a**) Group A. (**b**) Group B.

(**c**) Group C. (**d**) Group D.

(**e**) Type I. (**f**) Type II.

Figure 13. Shakedown threshold of dynamic stress amplitude.

The threshold curves of CSR^* are fitted by using the power function form, which can be expressed as

$$CSR^* = A{\sigma_3}^b \quad (8)$$

where A is mainly related to the variation amplitude of critical CSR with confining pressure, and b is related to the inclination of the threshold curve. For the typical high-speed railway subgrade fillers studied in this paper, the parameter values are shown in Table 3.

Table 3. Parameter values of the threshold curve of CSR (−).

Filler Type	Threshold	*A*	*b*
Group A of bottom layer	$CSR^*_{A–B}$	58.87	−0.78
	$CSR^*_{B–C}$	129.37	−0.80
Group B of bottom layer	$CSR^*_{A–B}$	76.63	−0.91
	$CSR^*_{B–C}$	140.41	−0.86
Group C of bottom layer	$CSR^*_{A–B}$	44.09	−0.70
	$CSR^*_{B–C}$	124.58	−0.78
Group D of bottom layer	$CSR^*_{A–B}$	49.24	−0.80
	$CSR^*_{B–C}$	107.62	−0.82
Type I of surface layer	$CSR^*_{A–B}$	38.45	−0.57
	$CSR^*_{B–C}$	246.97	−1.00
Type II of surface layer	$CSR^*_{A–B}$	59.79	−0.84
	$CSR^*_{B–C}$	126.84	−0.83

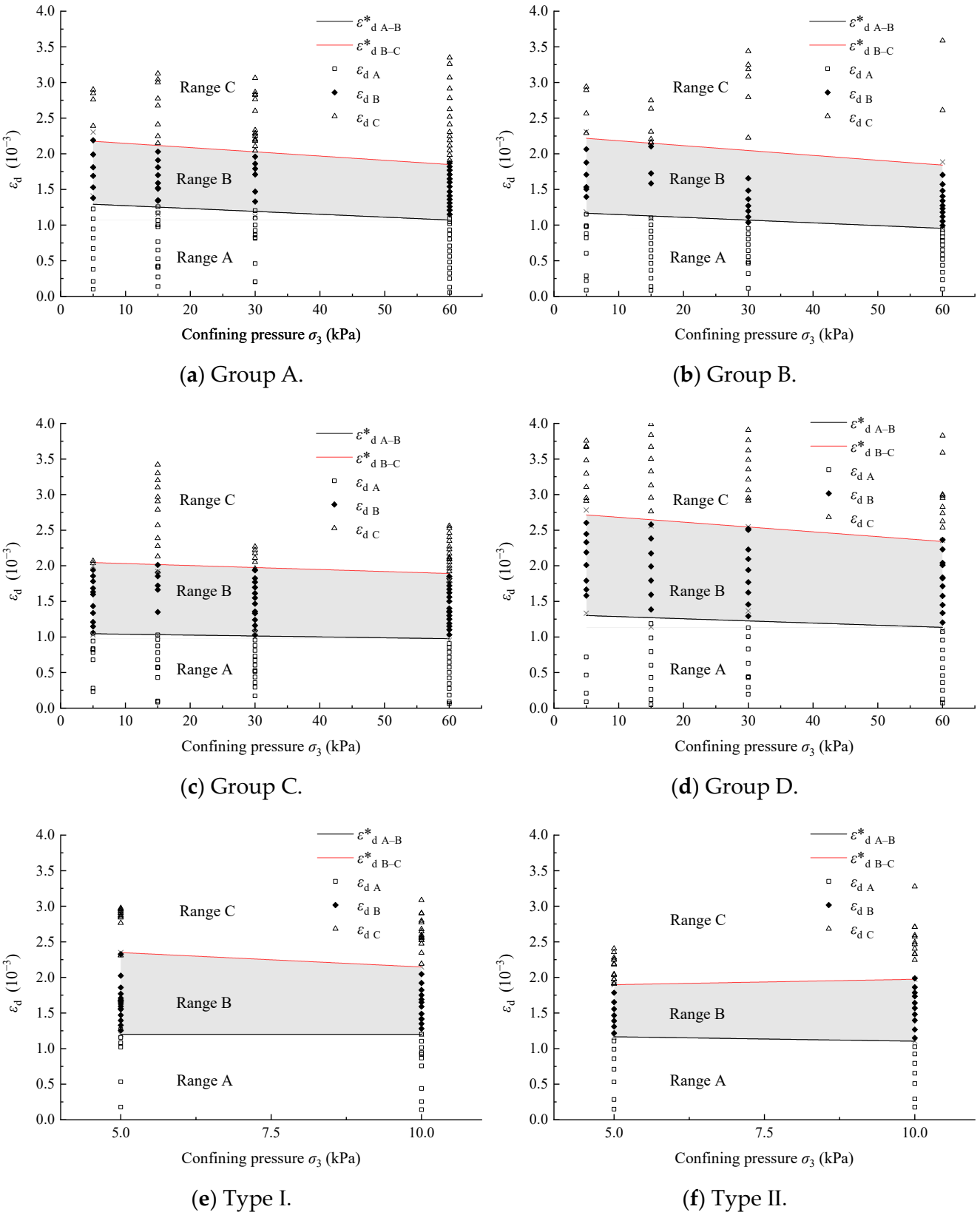
As shown in Figure 11, the curves of $CSR^*_{A–B}$ and $CSR^*_{B–C}$ showed a downward trend; however, the threshold of stress amplitude still increased with the increase in confining pressure. Taking the subgrade filler of Group A as an example, according to the conversion relationship in Equation (7), the thresholds of stress amplitude corresponding to $CSR^*_{A–B}$ and $CSR^*_{B–C}$ at σ_3 = 30 kPa were increased by about 46% and 15% compared with the values at σ_3 = 15 kPa, respectively. This indicated that the increase in confining pressure significantly enhanced the dynamic stability of subgrade fillers. Therefore, the filling near the surface layer of the high-speed railway subgrade was more likely to induce a reduction in stability and the accumulation of long-term deformation under a high external dynamic load. When designing subgrade structure, it is necessary to strictly control the filling and service quality of the surface filler to ensure that the confining pressure conditions and compactness of the filling location meet requirements.

Similarly, the threshold curves for dynamic strain amplitude $\varepsilon^*_{d\ A–B}$ and $\varepsilon^*_{d\ B–C}$ were analyzed, as shown in Figure 14.

The threshold curves of dynamic strain ε_d were fitted by using the linear function form, which is expressed as

$$\varepsilon_d = k\sigma_3 + \varepsilon_{d0} \quad (9)$$

where k is related to the change rate of the dynamic strain threshold with confining pressure, and ε_{d0} represents the dynamic strain threshold under the unconfined condition. The values of parameters are shown in Table 4.



(**a**) Group A. (**b**) Group B.

(**c**) Group C. (**d**) Group D.

(**e**) Type I. (**f**) Type II.

Figure 14. Shakedown threshold of dynamic strain amplitude.

Table 4. Parameter values of the threshold curve for ε_d (%).

Filler Type	Threshold	k	ε_{d0}	ε^*_d (10^{-3})
Group A of bottom layer	$\varepsilon^*_{d\ A–B}$	-4.03×10^{-6}	0.00131	0.119
	$\varepsilon^*_{d\ B–C}$	-5.94×10^{-6}	0.00221	0.203
Group B of bottom layer	$\varepsilon^*_{d\ A–B}$	-3.86×10^{-6}	0.00119	0.106
	$\varepsilon^*_{d\ B–C}$	-6.83×10^{-6}	0.00225	0.205
Group C of bottom layer	$\varepsilon^*_{d\ A–B}$	-1.26×10^{-6}	0.00105	0.101
	$\varepsilon^*_{d\ B–C}$	-2.80×10^{-6}	0.00206	0.198
Group D of bottom layer	$\varepsilon^*_{d\ A–B}$	-3.02×10^{-6}	0.00132	0.123
	$\varepsilon^*_{d\ B–C}$	-6.79×10^{-6}	0.00275	0.253
Type I of surface layer	$\varepsilon^*_{d\ A–B}$	-0.00×10^{-6}	0.00120	0.120
	$\varepsilon^*_{d\ B–C}$	-4.04×10^{-6}	0.00255	0.225
Type II of surface layer	$\varepsilon^*_{d\ A–B}$	-1.25×10^{-6}	0.00123	0.113
	$\varepsilon^*_{d\ B–C}$	1.53×10^{-6}	0.00182	0.194

The threshold curve of $\varepsilon^*_{d\ A–B}$ and $\varepsilon^*_{d\ B–C}$ tended to be linear, and the change rate was very small (<10^{-5}~10^{-6}), which indicated that the change in confining pressure had little effect on the shakedown threshold of dynamic strain. For the six types of high-speed railway subgrade fillers in this study, Table 4 shows that the values of $\varepsilon^*_{d\ A–B}$ were approximately in the range of 0.10~0.12% and the value of $\varepsilon^*_{d\ B–C}$ was about 0.20~0.25%. In order to ensure the long-term stability of high-speed railway subgrade, it is necessary to avoid exceeding the threshold $\varepsilon^*_{d\ B–C}$ and to control the dynamic strain of subgrade filler below the threshold $\varepsilon^*_{d\ A–B}$ as far as possible.

4.3. Control Threshold for Dynamic Shakedown Design of High-Speed Railway Subgrade

Considering the shakedown characteristics of the filler, the dynamic stress σ_{di} and dynamic strain ε_{di} of the i-th layer of the subgrade should be less than the shakedown thresholds during the design of high-speed railway subgrade, as shown in Equations (10) and (11).

$$\begin{cases} \sigma_{di} \le n \cdot CSR^*_{A-B} \cdot \sigma_{3i} = 1/n \cdot CSR^*_{A-B} \cdot k_i \cdot \rho_i \cdot h_i \\ \sigma_{di} \le CSR^*_{B-C} \cdot \sigma_{3i} = CSR^*_{B-C} \cdot k_i \cdot \rho_i \cdot h_i \end{cases} \tag{10}$$

$$\begin{cases} \varepsilon_{di} \le 1/n \cdot \varepsilon^*_{d\ A-B} \\ \varepsilon_{di} \le \varepsilon^*_{d\ B-C} \end{cases} \tag{11}$$

where ρ_i, h_i, and k_i are the density, thickness, and earth pressure coefficient of subgrade filler corresponding to the i-th layer, respectively, and the confining pressure σ_{3i} can be calculated; n is the safety factor proposed according to the design requirements of different control levels, considering the deformation stability. With stricter requirements for deformation control in a design, the value of n increases.

5. Conclusions

Based on shakedown theory and adopting an energy perspective, this paper investigated the characteristics of plastic strain accumulation, cyclic stress–strain hysteresis, and the evolution of dissipation energy in six types of typical coarse-grained soil fillings used in subgrade construction. A criterion for identifying the shakedown critical state based on equivalent unit volume dissipation energy is proposed, along with a methodology for determining the corresponding control threshold. Different from the traditional method, the method proposed in this paper was more accurate in evaluating the shakedown states. It established a relationship among long-term deformation trends, the shakedown critical

state, and dissipation energy. This method offers the advantage of comprehensively considering both the magnitude and the trend of strain energy dissipation. The findings of this research can provide a theoretical foundation for the shakedown design of high-speed railway subgrades.

The main results are as follows:

(1) The three deformation development modes of high-speed railway subgrade fillers corresponded to distinct shakedown characteristics, strain accumulation rates, and variations in dissipated energy.

Range A (Plastic Shakedown): the strain accumulation rate decreased rapidly with increasing permanent deformation, while the dissipated energy per unit volume stabilized at a low level.

Range B (Plastic Creep): the strain accumulation rate declined gradually, accompanied by a slight increase in dissipated energy per unit volume after a certain number of cycles.

Range C (Incremental Collapse): the strain accumulation rate remained elevated, with substantial fluctuations in the dissipated energy per unit volume as the cycle number increased.

(2) A criterion of shakedown state based on dissipated energy per unit volume was proposed. For the six types of typical high-speed railway subgrade fillers, the values of λ_{A-B} and λ_{B-C} were observed to fall within the ranges of 0.01 to 0.015 kJ/m^3; and 0.05 to 0.08 kJ/m^3;, respectively.

(3) The thresholds of CSR^* and ε^*_d of the six types of high-speed railway subgrade fillers have been established. It was found that the critical CSR decreased as the confining pressure increased, while the threshold for dynamic stress shakedown exhibited an upward trend. Conversely, the critical threshold for dynamic strain was relatively unaffected by changes in confining pressure. In this study, the values of $\varepsilon^*_{d\,A-B}$ and $\varepsilon^*_{d\,B-C}$ were approximately in the range of 0.10% to 0.12% and 0.20% to 0.25%, respectively.

(4) Control thresholds for dynamic shakedown design of high-speed railway subgrade were proposed. By regulating the thresholds for dynamic stress and dynamic strain, the subgrade can be maintained in a shakedown state, thereby preventing long-term accumulated deformation and incremental collapse. These results offer valuable theoretical support for the shakedown design of high-speed railway subgrades.

This study primarily focuses on conducting experiments and analyzing data related to the types and compaction requirements of high-speed railway subgrade fillers as specified in current standards. The critical shakedown conditions and design thresholds proposed herein have limitations when applied to a broader range of filler types, varying compaction levels, and different moisture conditions. Therefore, further experimental analysis is necessary, to enhance the applicability of these results across diverse scenarios.

Author Contributions: Conceptualization, Z.B. and Y.Y.; Methodology, Z.B., D.C. and K.S.; Software, K.S. and M.O.; Validation, Z.B. and H.Y.; Formal analysis, D.C., H.Y. and K.S.; Investigation, Z.B., D.C. and K.S.; Writing—original draft, Z.B.; Writing—review & editing, Y.Y.; Supervision, Y.Y. All authors have read and agreed to the published version of the manuscript.

Funding: This research was funded by the National Natural Science Foundation of China (Grant No. 52308471), the Science and Technology Research and Development Plan of China State Railway Group Co., Ltd. (K2022G060), the Research Projects of China Academy of Railway Sciences Group Co., Ltd. (2021YJ024), and the Tencent Science Exploration Award in 2022.

Institutional Review Board Statement: Not applicable.

Informed Consent Statement: Not applicable.

Data Availability Statement: Not applicable.

Conflicts of Interest: Authors Zongqi Bi, Degou Cai, Hongye Yan, Mingzhe Ouyang and Ke Su were employed by the companies Railway Engineering Research Institute, China Academy of Railway Sciences Corporation Limited and State Key Laboratory for Track Technology of High-Speed Railway, China Academy of Railway Sciences Corporation Limited. Author Yangsheng Ye was employed by the companies State Key Laboratory for Track Technology of High-Speed Railway, China Academy of Railway Sciences Corporation Limited and China State Railway Group Corporation Limited. All authors declare that the research was conducted in the absence of any commercial or financial relationships that could be construed as a potential conflict of interest.

Nomenclature

Abbreviations

BP	backpropagation
TPM	thermo-parameter method
FEM	finite element method
CSR	cyclic stress ratio

Indices

i	the index of numbers
d	the index of dynamic variables
e	the index of elastic variables
p	the index of plastic variables

Parameters

Δl_{d}	the subsequent amplitude increment of each level
ΔN	the number of load cycles of each level
A_{s}	the area of the specimen subjected to axial force
m	the maximum cycle number
A	the variation amplitude of critical *CSR* with confining pressure
b	the inclination of the threshold curve
k	the change rate of the dynamic strain threshold with confining pressure
$\varepsilon_{\mathrm{d0}}$	the dynamic strain threshold under the unconfined condition
n	safety factor
ρ_i	the density of the subgrade filler
h_i	the thickness of the subgrade filler
k_i	the earth pressure coefficient of the subgrade filler

Variables

σ_3	confining pressure
σ_{d}	dynamic stress
ε^p	cumulative strain
σ	the stress of the loading section
ε	the strain of the loading section
σ'	the stress of the unloading section
ε'	the strain of the unloading section
σ_i	the stress of segment i after discretization
ε_i	the strain of segment i after discretization
$\dot{\varepsilon}_{ij}^{*p}$	plastic strain rate
σ_{ij}^{*}	stress associated with $\dot{\varepsilon}_{ij}^{*p}$ through the plastic flow law
$\lambda_{\mathrm{A-B}}$	critical values of equivalent dissipated energy per unit volume between Range A and B
$\lambda_{\mathrm{B-C}}$	critical values of equivalent dissipated energy per unit volume between Range B and C
$CSR^*_{\mathrm{A-B}}$	the critical cyclic stress ratio of Range A–B
$CSR^*_{\mathrm{B-C}}$	the critical cyclic stress ratio of Range B–C
N	the number of cycles
$l_{\mathrm{d,i}}$	the ith level load amplitude
U^{d}	dissipated energy per unit volume
U	total unit volume energy
U^{e}	unit volume elastic energy
$P_a(t)$	the action of the external force
$\dot{u}_a^*(t)$	kinematically admissible velocity field
$\overline{U}_{\mathrm{eq}}^{\mathrm{d}}$	equivalent dissipated energy per unit volume
$\overline{U}^{\mathrm{d}}$	the mean value of U^{d}
U_m^{d}	the final U^{d} corresponding to the maximum cycle number m
$U_{m/10}^{\mathrm{d}}$	the U^{d} corresponding to the representative cycle number $m/10$
$\overline{U}_{\mathrm{eq,Amax}}^{\mathrm{d}}$	the max value of $\overline{U}_{\mathrm{eq}}^{\mathrm{d}}$ in Range A
$\overline{U}_{\mathrm{eq,Bmin}}^{\mathrm{d}}$	the min value of $\overline{U}_{\mathrm{eq}}^{\mathrm{d}}$ in Range B
$\overline{U}_{\mathrm{eq,Bmax}}^{\mathrm{d}}$	the max value of $\overline{U}_{\mathrm{eq}}^{\mathrm{d}}$ in Range B
$\overline{U}_{\mathrm{eq,Cmin}}^{\mathrm{d}}$	the min value of $\overline{U}_{\mathrm{eq}}^{\mathrm{d}}$ in Range C

References

1. Mylonakis, G.; Gazetas, G. Seismic Soil-Structure Interaction: Beneficial or Detrimental? *J. Earthq. Eng.* **2000**, *4*, 277–301. [CrossRef]
2. Savvides, A.-A. A Parametric Study of the Dynamic Soil–Structure Interaction for Shear Vulnerable Structures with Nonlinear Finite Element Modelling. *Geotechnics* **2024**, *4*, 693–717. [CrossRef]
3. Guo, H.; Su, Q.; Li, T.; Zhang, Q.; Nadakatti, M.M.; Yan, H.; Chen, F. Field Comprehensive Testing and Study on New Subgrade Structure of High-Speed Railway in Diatomaceous Earth Region. *Sustainability* **2023**, *15*, 6912. [CrossRef]

4. Wang, J.; Han, J.; Chen, J.; Ding, G.; Feng, G.; Liu, T.; Guo, B. Experimental and Numerical Study on the Dynamic Response of a Superthick Backfill Subgrade under High-Speed Railway Loading: A Case Study of Qianjiang–Zhangjiajie–Changde Railway. *J. Constr. Eng. Manag.* **2022**, *148*, 05022014. [CrossRef]
5. Morgan, J.R. The Response of Granular Materials to Repeated Loading. In Proceedings of the 3rd Australian Road Research Board Conference, Sydney, Australia, 5–9 September 1966; Australian Road Research Board: Port Melbourne, Australia, 1966; pp. 1178–1192.
6. Barksdale, R.D. Laboratory Evaluation of Rutting in Base Course Materials. In *Proceeding of 3rd International Conference on the Structural Design of Asphalt Pavements*; Michigan State University: Ann Arbor, MI, USA, 1972; pp. 161–174.
7. Behzadi, G.; Yandell, W. Determination of Elastic and Plastic Subgrade Soil Parameters for Asphalt Cracking and Rutting Prediction. *Transp. Res. Rec. J. Transp. Res. Board* **1996**, *1540*, 97–104. [CrossRef]
8. Muhanna, A.S.; Rahman, M.S.; Lambe, P.C. Resilient Modulus Measurement of Fine-Grained Subgrade Soils. *Transp. Res. Rec. J. Transp. Res. Board* **1999**, *1687*, 3–12. [CrossRef]
9. Ye, Y. Study on Deformation Characteristics of Saturated Soft Clay Under Unidirectional Cyclic Load. Ph.D. Thesis, China Academy of Railway Sciences, Beijing, China, 1996.
10. Lentz, R.; Baladi, G. Constitutive Equation for Permanent Strain of Sand Subjected to Cyclic Loading. *Transp. Res. Rec. J. Transp. Res. Board* **1981**, *810*, 50–54.
11. Qiu, Y.J. Permanent Deformation of Subgrade Soils Laboratory Investigation and Application in Mechanistic-Based Pavement Design. Ph.D. Thesis, University of Arkansas, Fayetteville, AR, USA, 1998.
12. Seed, H.; Chan, C.; Monismith, C. Effects of Repeated Loading on the Strength and Deformation of Compacted Clay. *Highw. Res. Rec.* **1955**, *34*, 541–558.
13. Brown, S.F.; Hyde, A.F. *Significance of Cyclic Confining Stress in Repeated Load Triaxial Testing of Granular Material*; Transportation Research Board: Washington, DC, USA, 1975.
14. Wang, T.; Zhang, F.; Song, H.; Bu, J.; Yin, Z. Experimental Study on Dynamic and Static Mechanical Properties of Coarse-grained Soil Filled in High-speed Railway Subgrade. *J. China Railw. Soc.* **2022**, *44*, 127–135.
15. Heath, D.L.; Waters, J.M.; Shenton, M.J.; Sparrow, R.W. Design of Conventional Rail Track Foundations. *Proc. Inst. Civ. Eng.* **1972**, *51*, 251–267. [CrossRef]
16. Cai, Y.; Cao, X. Study of the Critical Dynamic Stress and Permanent Strain of the Subgrade-Soil under the Repeated Load. *J. Southwest Jiaotong Univ.* **1996**, *31*, 1–4.
17. Wang, L.; Xie, X.; Ba, H. Critical Stress and Plastic Deformation of Graded Aggregate Material Under Long-term Dynamic Repeat Load. *J. Tongji Univ. (Nat. Sci.)* **2010**, *38*, 1293–1297.
18. Minassian, G.H. Behavior of Granular Materials Under Cyclic and Repeated Loading. Ph.D. Thesis, University of Alaska, Fairbanks, AK, USA, 2003.
19. Jiao, G.; Zhao, S.; Ma, W. Experimental Study of the Dynamic Characteristics of Warm-Frozen Silt after Freeze-Thaw Cycles under Cyclic Loading. *China Civ. Eng. J.* **2010**, *43*, 107–113.
20. Nie, R.; Du, S.; Ruan, B.; Zhang, X. Experimental Study on Cumulative Plastic Strain and Critical Dynamic Stress of Fine-grained Soil Filler Considering Intermittent Load. *J. China Railw. Soc.* **2021**, *43*, 98–108.
21. Luo, Q.; Liu, G.; Zhang, L.; Jiang, L.-w.; Xiong, Y. Characteristics of Cumulative Deformation Evolution State of Subgrade Filler under Cyclic Loading and Experimental Verification. *J. China Railw. Soc.* **2016**, *38*, 110–116.
22. Liu, G. Study on the Design Method for Subgrade of High-Speed Railway Base on the Long-Term Cumulative Deformation Evolution State Controlling. Ph.D. Thesis, Southwest Jiaotong University, Chengdu, China, 2013.
23. Ye, Y.; Cai, D.; Geng, L.; Yan, H.; Yao, J.; Chen, F. Constitutive Model for Cyclic Densification of Coarse-Grained Soil Filler for High-Speed Railway Subgrade Considering Particle Breakage. *China Railw. Sci.* **2020**, *41*, 11–20. [CrossRef]
24. Zhang, Q.; Han, Z.; Lyu, B. Structural Analysis and Design Method for Subgrade Bed of High-Speed Railway. *China Railw. Sci.* **2005**, *26*, 53–57. [CrossRef]
25. Melan, E. Zur Plastizität des Räumlichen Kontinuums. *Ing.-Arch.* **1938**, *9*, 116–126. [CrossRef]
26. Maier, G. Shakedown Theory in Perfect Elastoplasticity with Associated and Nonassociated Flow-Laws: A Finite Element, Linear Programming Approach. *Meccanica* **1969**, *4*, 250–260. [CrossRef]
27. Ceradini, G. Dynamic Shakedown in Elastic-Plastic Bodies. *J. Eng. Mech. Div.* **1980**, *106*, 481–499. [CrossRef]
28. Polizzotto, C. Dynamic Shakedown of Elastic-Plastic Solids for a Set of Alternative Loading Histories. *Int. J. Non-Linear Mech.* **1984**, *19*, 363–371. [CrossRef]
29. Sharp, R.W.; Booker, J.R. Shakedown of Pavements under Moving Surface Loads. *J. Transp. Eng.* **1984**, *110*, 1–14. [CrossRef]
30. Wang, F. Numerical Methods of Shakedown Analysis of Soil Structure and Its Applications in Evaluation of Bearing Capacity of Offshore Foundations. Ph.D. Thesis, University of Technology, Dalian, China, 2002.
31. Arvin, M.R.; Askari, F.; Farzaneh, O. Seismic Behavior of Slopes by Lower Bound Dynamic Shakedown Theory. *Comput. Geotech.* **2012**, *39*, 107–115. [CrossRef]

32. Wang, J.; Liu, S.; Yang, W.B. Dynamics Shakedown Analysis of Slab Track Substructures with Reference to Critical Speed. *Soil Dyn. Earthq. Eng.* **2018**, *106*, 1–13. [CrossRef]
33. Werkmeister, S.; Dawson, A.R.; Wellner, F. Permanent Deformation Behavior of Granular Materials and the Shakedown Concept. *Transp. Res. Rec. J. Transp. Res. Board* **2001**, *1757*, 75–81. [CrossRef]
34. Chen, W.B.; Feng, W.Q.; Yin, J.H.; Borana, L.; Chen, R.P. Characterization of Permanent Axial Strain of Granular Materials Subjected to Cyclic Loading Based on Shakedown Theory. *Constr. Build. Mater.* **2019**, *198*, 751–761. [CrossRef]
35. Xiao, Y.J.; Zhang, Z.; Chen, L.X.; Zheng, K. Modeling Stress Path Dependency of Cyclic Plastic Strain Accumulation of Unbound Granular Materials under Moving Wheel Loads. *Mater. Des.* **2018**, *137*, 9–21. [CrossRef]
36. Xiao, J.H.; Zhang, D.; Wei, K.; Luo, Z. Shakedown Behaviors of Railway Ballast under Cyclic Loading. *Constr. Build. Mater.* **2017**, *155*, 1206–1214. [CrossRef]
37. Zheng, K.Y.; Xiao, Y.J.; Wang, M.; Wang, B.; Yan, J.L.; Chen, X.B.; Ye, X.Y. Permanent Deformation Characteristics and Shakedown Analysis of Coarse-Grained Embankment Materials under Moving Wheel Loads. *Chin. J. Rock Mech. Eng.* **2020**, *39*, 1930–1943.
38. Wang, S.; Li, X.; Ti, Y.; Zhang, X.; Yin, T.; Wang, R.; Jiang, X.; Su, Z.; Hao, J. Investigation on shakedown response-behavior of thawed subgrade soils under long-term traffic loading. *Front. Earth Sci.* **2024**, *12*, 1361283. [CrossRef]
39. Wang, K.; Zhuang, Y. Characterizing the permanent deformation Response-Behavior of subgrade material under cyclic loading based on the shakedown theory. *Constr. Build. Mater.* **2021**, *311*, 125325. [CrossRef]
40. Wang, K.; Chen, Z.; Wang, Z.; Chen, Q.; Ma, D. Critical Dynamic Stress and Cumulative Plastic Deformation of Calcareous Sand Filler Based on Shakedown Theory. *J. Mar. Sci. Eng.* **2023**, *11*, 195. [CrossRef]
41. Liu, G.; Zhao, M.; Luo, Q.; Lu, R. Characterization of permanent deformation properties of densely-compacted unbound granular materials subjected to cyclic loading. *Sci. Rep.* **2023**, *13*, 3731. [CrossRef] [PubMed]
42. Liu, G.; Zhao, M.; Luo, Q.; Zhou, J. A New Approach for Classifying the Permanent Deformation Properties of Granular Materials under Cyclic Loading. *Materials* **2023**, *16*, 2141. [CrossRef]
43. Martins, L.A.; Correia, A.A.S.; Venda Oliveira, P.J.; Lemos, L.J. Using the shakedown theory to study the cyclic behaviour of an unreinforced and fibre-reinforced stabilized soft soil. *Int. J. Geotech. Eng.* **2024**, *18*, 332–343. [CrossRef]
44. Indraratna, B.; Nguyen, T.T.; Atapattu, S.; Ngo, T.; Rujikiatkamjorn, C. Subgrade soil response to rail loading: Instability mechanisms, causative factors, and preventive measures. *Transp. Geotech.* **2024**, *46*, 101267. [CrossRef]
45. Zhang, D.; Cui, K.; Li, Q.; Yang, S.; Li, P.; Wu, Z.; Li, X.; Xie, J. Plastic shakedown limit of geosynthetic reinforced coarse-grained soil: Experiments and prediction model. *Geotext. Geomembr.* **2024**, *52*, 813–827. [CrossRef]
46. Li, Y.; Nie, R.; Guo, Y.; Wang, C.; Wang, Q.; Yue, Z. Resilient deformation characteristics of subgrade silty filler under intermittent train loading. *Transp. Geotech.* **2023**, *40*, 100952. [CrossRef]
47. Zhai, B.; Xu, F.; Leng, W.; Xu, F.; Zhang, S.; Ye, X.; Leng, H. Critical dynamic stress and shakedown limit criterion of coarse-grained subgrade soil. *Transp. Geotech.* **2020**, *23*, 100354. [CrossRef]
48. Xu, F.; Zhai, B.; Leng, W.; Ye, X.Y.; Zhang, Q.S.; Zhao, C. Study on Critical Dynamic Stress of Coarse-grained Soil Based on Large-Scale Dynamic Triaxial Test and Neural Network. *J. China Railw. Soc.* **2023**, *45*, 119–127.
49. Bi, Z.; Ye, Y.; Gong, Q.; Cai, D.; Yan, H.; Wei, S.; Yao, J. An Improved Thermo-Parameters Method for Dynamic Shakedown Analysis of Railway Subgrade. *Transp. Geotech.* **2022**, *33*, 100657. [CrossRef]
50. Lei, H.; Qian, J.; Dai, Y.; Wang, Y. Effects of pavement roughness on shakedown limits under moving traffic loadings. *IOP Conf. Ser. Earth Environ. Sci.* **2024**, *1332*, 012005. [CrossRef]
51. *TB 10001-2016*; National Railway Administration of the People's Republic of China. Code for Design of Railway Earth Structure. China Railway Publishing House: Beijing, China, 2016.
52. Mei, H.; Nie, R.; Leng, W.; Li, Y.; Chen, X. Characterisation of Permanent Deformation Behaviour of Silt by Using both Single-Stage and Multi-Stage Repeated Load Triaxial Tests Considering Time Intermittent Effect. *J. China Railw. Soc.* **2021**, *43*, 94–104.
53. Mei, H.H.; Leng, W.M.; Nie, R.S.; Liu, W.; Chen, C.; Wu, X. Random Distribution Characteristics of Peak Dynamic Stress on the Subgrade Surface of Heavy-Haul Railways Considering Track Irregularities. *Soil Dyn. Earthq. Eng.* **2019**, *116*, 205–214. [CrossRef]
54. Zhao, C.; Wu, K.; Li, S.; Zhao, J. Energy Characteristics and Damage Deformation of Rock Subjected to Cyclic Loading. *Chin. J. Geotech. Eng.* **2013**, *35*, 890–896.
55. Xie, J.; Feng, W.; Hu, Y.; Wu, G.; Qiao, Y. An Analysis of the Mechanical Properties and Energy Characteristics of Damage Deformation of Mudstone under Natural and Saturated States. *Hydrogeol. Eng. Geol.* **2016**, *43*, 66–72,78.
56. Koiter, W.T. *General Theorems for Elastic-Plastic Solids: Progress in Solid Mechanics*; North-Holland Publishing Co.: Amsterdam, The Netherlands, 1960.
57. Zhang, J.; Wang, D.; Wu, W.; Chen, Q. Application of Kinematic Shakedown Theorem in Shakedown Analysis of Pavement Structures. *J. Harbin Inst. Technol.* **2012**, *44*, 119–123.

Disclaimer/Publisher's Note: The statements, opinions and data contained in all publications are solely those of the individual author(s) and contributor(s) and not of MDPI and/or the editor(s). MDPI and/or the editor(s) disclaim responsibility for any injury to people or property resulting from any ideas, methods, instructions or products referred to in the content.